

Rethinking Medical Anomaly Detection in Brain MRI: An Image Quality Assessment Perspective

Zixuan Pan

Computer Science and Engineering
University of Notre Dame
Notre Dame, USA
zpan3@nd.edu

Jun Xia

Computer Science and Engineering
University of Notre Dame
Notre Dame, USA
jxia4@nd.edu

Zheyu Yan

Computer Science and Engineering
University of Notre Dame
Notre Dame, USA
zyan2@nd.edu

Guoyue Xu

Aerospace and Mechanical Engineering
University of Notre Dame
Notre Dame, USA
gxu3@nd.edu

Yawen Wu

Computer Science and Engineering
University of Notre Dame
Notre Dame, USA
yawen.wu@pitt.edu

Zhenge Jia

Computer Science and Technology
Shandong University
Shandong, China
zhengejia@sdu.edu.cn

Jianxu Chen

Leibniz-Institut für Analytische Wissenschaften - ISAS e.V.
Dortmund, Germany
jianxu.chen@isas.de

Yiyu Shi

Computer Science and Engineering
University of Notre Dame
Notre Dame, USA
yshi4@nd.edu

Abstract—Reconstruction-based methods, particularly those leveraging autoencoders, have been widely adopted to perform anomaly detection in brain MRI. While most existing works try to improve detection accuracy by proposing new model structures or algorithms, we tackle the problem through image quality assessment, an underexplored perspective in the field. We propose a fusion quality loss function that combines Structural Similarity Index Measure loss with ℓ_1 loss, offering a more comprehensive evaluation of reconstruction quality. Additionally, we introduce a data pre-processing strategy that enhances the average intensity ratio (AIR) between normal and abnormal regions, further improving the distinction of anomalies. By fusing the aforementioned two methods, we devise the image quality assessment (IQA) approach. The proposed IQA approach achieves significant improvements ($>10\%$) in terms of Dice coefficient (DICE) and Area Under the Precision-Recall Curve (AUPRC) on the BraTS21 (T2, FLAIR) and MSULB datasets when compared with state-of-the-art methods. These results highlight the importance of invoking the comprehensive image quality assessment in medical anomaly detection and provide a new perspective for future research in this field. The code is available at <https://github.com/zx-pan/MedAnomalyDetection-IQA>.

Index Terms—Anomaly detection, Autoencoders, DDPM, Image quality assessment

I. INTRODUCTION

For decades, deep learning methods [1], [2] have been widely used to assist radiologists in disease recognition, such as detecting tumors from brain MRI scans. Traditional supervised learning approaches, however, require a large amount of labeled data (e.g., tumor segmentation masks), which are often difficult to obtain for medical images. To address this challenge, many self-supervised, semi-supervised, and weakly

supervised learning methods [3], [4] have been developed. These methods effectively utilize both limited labeled data and abundant unlabeled data. Among these approaches, framing the disease recognition task as an anomaly detection problem has gained popularity. This type of method trains solely on unannotated normal images (e.g., MRI scans of healthy brains), enabling the identification of abnormalities (e.g., tumor segmentation) without extensive manual labeling.

Reconstruction-based methods, such as autoencoders (AEs) and their variants, have shown great promise in medical anomaly detection. These methods are trained to reconstruct original images from corrupted versions, with the assumption that anomalies are harder to reconstruct than normal regions. During inference, the difference between the reconstructed and original test images indicates the anomaly level for each pixel. Consequently, abnormal areas exhibit higher reconstruction errors, detectable through post-processing techniques (e.g., binarization with a threshold).

However, standard AEs and variational autoencoders (VAEs) often produce blurry reconstructions, leading to sub-optimal anomaly detection performance. To enhance these models, various improvements have been proposed, such as adding spatial latent dimensions [5], incorporating skip connections [6], or developing denoising autoencoders (DAEs) [7]. Research has also highlighted that simplex noise generally outperforms Gaussian noise in DAE-based anomaly detection [7], [8].

While these work takes much efforts in carefully designing the models and algorithms, the importance of the metrics used to evaluate reconstructions is often overlooked, with most

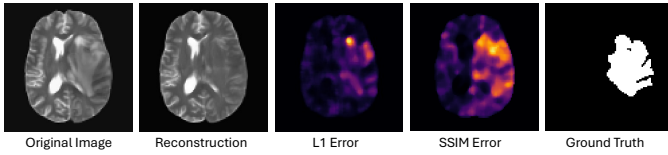


Fig. 1. Visualization of the anomaly maps generated by ℓ_1 loss and SSIM loss from the same reconstruction. Calculating the reconstruction discrepancy with L1-metric cannot flag the large tumor area, while calculating with SSIM, from the same reconstruction, could identify the tumor area significantly better.

approaches defaulting to ℓ_1 loss. In contrast, we revisit the problem of reconstruction-based anomaly detection in brain MRI from an image quality assessment (IQA) perspective, an underexplored aspect in this field. Our intuition is based on the observation that simply changing the way the reconstruction residuals are calculated can significantly improve anomaly detection performance. As shown in Fig. 1, even with the same reconstruction, using Structural Similarity Index Measure (SSIM) loss to calculate the anomaly map can detect the anomalies that the commonly used ℓ_1 loss might miss.

Based on the above observations, we argue that metrics beyond ℓ_1 are essential for a more comprehensive assessment of reconstructions during the training and inference phases of anomaly detection. We propose a fusion quality loss that combines SSIM loss with the widely used ℓ_1 loss. This combined loss function evaluates the reconstruction based on intensity (subtractive from ℓ_1 and divisive from SSIM), contrast, and structure similarity, capturing the strength of both error functions.

Evaluating reconstruction quality beyond just pixel-wise intensity introduces a higher level view, making subtle variations in different regions more impactful in the final assessment, comparing to existing anomaly detection solutions. In this situation, the inherent characteristics of images from a semantic perspective becomes increasingly important for optimizing anomaly detection performance, therefore necessitates commensurate pre-processing steps tailored to these expanded metrics. Since we introduce divisive metrics from SSIM, it is important to amplify the divisive discrepancies between anomalies and normal regions. To this end, we propose a pre-processing strategy to consistently enhance the average intensity ratio (AIR) between normal and abnormal regions, thereby improving the overall effectiveness of the model.

We refer to our final approach, which combines the fusion quality loss and AIR enhancement pre-processing strategy, as the IQA approach. We evaluate its effectiveness on several commonly used datasets by applying it to a baseline model.

We summarize our main contributions as follows:

- **Incorporation of SSIM Loss:** To the best of our knowledge, we are the first to incorporate SSIM loss alongside ℓ_1 loss for both training and inference in brain MRI anomaly detection.
- **Pre-processing Strategy:** We propose a simple yet effective dataset pre-processing strategy to enhance AIR and validate its effectiveness both theoretically and empiri-

cally.

- **Comprehensive experiments:** Our results show that our method achieves relative improvements in DICE of up to 15.86% for BraTS21 T2, 21.41% for MSLUB, 30.82% for BraTS21 FLAIR, and 5.27% for BraTS21 T1-CE compared to state-of-the-art (SOTA) baselines.
- **Image quality assessment perspective:** We investigate brain MRI anomaly detection from an image quality assessment perspective and achieve state-of-the-art performance on the BraTS21 (T2, FLAIR) and MSLUB datasets. Our approach opens a new door in the community for studying medical image anomaly detection.

II. RELATED WORK

In recent years, reconstruction-based methods using autoencoders (AEs) and their variants have become increasingly popular for medical anomaly detection. These models are trained to reconstruct healthy images, and the reconstruction error is used as an anomaly score. However, the tendency of AEs and VAEs to produce blurry reconstructions can limit their effectiveness in detecting anomalies [9]. To address this, various advanced AE models have been explored. [10] proposes using vector-quantized VAEs that improve discrete feature representation. [11] introduces adversarial autoencoders to enhance generative quality through adversarial training. [7] uses denoising autoencoders (DAE) to improve image clarity by adding skip connections and performs denoising task during training.

Other than AE-based methods, generative adversarial networks (GANs) have also been applied to anomaly detection tasks. AnoGAN [12], the first GAN-based approach for this task, identifies anomalies in medical images by comparing test images with their GAN-generated healthy counterparts in pixel space. However, AnoGAN requires extensive inference time due to its reliance on numerous back-propagation iterations. To improve inference speed, f-AnoGAN [13] uses an encoder with a Wasserstein GAN for faster mapping to latent space. Despite these improvements, GANs still face stability issues during training and often fail to maintain anatomical coherence, leading to problems like mode collapse [9].

Denoising diffusion probabilistic models (DDPM) have recently gained attention as a robust method for anomaly detection in brain MRI. anoDDPM [8] was the first to apply DDPM in this context, proposing the use of simplex noise to replace Gaussian noise. Building on this, pDDPM [14] improved anomaly detection performance by adopting a patch-based DDPM approach, where noise is added to patches while the rest of the image remains uncorrupted and serves as a condition. This technique enhances brain MRI reconstruction by incorporating global context information about individual brain structures and appearances. Further extending this concept, mDDPM [15] applied the patch-based approach to the frequency domain, yielding additional improvements.

While much of work in the anomaly detection has focused on designing architectures and algorithms, some studies have investigated different ways of measuring discrepancies. For

instance, [16] applies SSIM loss for industrial defect detection, and replacing the ℓ_2 loss. [17] proposed calculating SSIM loss in latent space instead of pixel space, and [18] designed an ensembled SSIM approach for anomaly score calculation.

In summary, existing work in medical anomaly detection has either utilized SSIM loss in latent space or applied it only during inference for anomaly score calculation. We are the first to incorporate SSIM loss for both training and inference in the medical anomaly detection problem, achieving state-of-the-art performance on several commonly used datasets.

III. METHOD

In this section, we will first sketch the overall framework of reconstruction based anomaly detection and then the core concept of denoising diffusion probabilistic models, which will be the basic our method builds upon. After that, we will introduce our proposed *Fusion Quality Loss* and *Average Intensity Ratio Enhancement*, the two major findings after revisiting the brain MRI anomaly detection from an image quality assessment (IQA) perspective. An overview of our final reconstruction-based anomaly detection framework is shown in Fig. 2.

A. Anomaly detection with pDDPM

1) *Reconstruction-based anomaly detection*: Given a normal dataset $X_n = \{x_1^n, x_2^n, \dots, x_N^n\}$, a reconstruction-based anomaly detection method usually trains a model $f_\theta(\cdot)$ to restore the original x_i^n from a disturbed one $x_i^{n'}$ and expect the reconstruction \hat{x}_i^n to be as close to x_i^n as possible.

$$\min_{\theta} \frac{1}{N} \sum_{i=1}^N L_{train}(x_i^n, \hat{x}_i^n = f_\theta(x_i^{n'})), \quad (1)$$

where L_{train} is a function to measure the reconstruction quality.

During Inference, we denote the test dataset with anomalies as $X_a = \{x_1^a, x_2^a, \dots, x_M^a\}$. For any test image $x_j^a \in X_a$, we first degrade it to $x_j^{a'}$, and then use the well-trained reconstruction model $f_{\theta^*}(\cdot)$ to get the reconstruction \hat{x}_j^a . The pixel-wise anomaly score map Λ_j is defined by the reconstruction error:

$$\Lambda_j = L_{test}(x_j^a, \hat{x}_j^a = f_{\theta^*}(x_j^{a'})), \quad (2)$$

where higher values correspond to larger reconstruction errors, indicating higher probability of being abnormal. L_{test} serves the same purpose of assessing the reconstructed image as L_{train} , though it may use a different function. A threshold is then applied to Λ_j for binarization post-processing to obtain the final anomaly segmentation.

2) *pDDPM*: Denoising Diffusion Probabilistic Models (DDPMs) are a class of generative models which have recently gained significant popularity. The training of DDPMs consists of a Markovian forward process (the *diffusion process*) and a reverse sampling procedure (the *reverse process*). In the *diffusion process* guided by a noise schedule $\{\beta_1, \beta_2, \dots, \beta_T\}$, the image x_0 is degraded to the noisy image x_t by

$$\begin{aligned} q(x_t|x_0) &:= \mathcal{N}(x_t; \sqrt{\bar{\alpha}_t}x_0, (1 - \bar{\alpha}_t)I), \\ x_t &= \sqrt{\bar{\alpha}_t}x_0 + \epsilon\sqrt{1 - \bar{\alpha}_t}, \epsilon \sim \mathcal{N}(0, I) \end{aligned} \quad (3)$$

where $\alpha_t := 1 - \beta_t$ and $\bar{\alpha}_t := \prod_{s=1}^t \alpha_s$.

[19] show that, in the *reverse process*, we can model the distribution $p_\theta(x_{t-1}|x_t)$ of x_{t-1} given x_t as a diagonal Gaussian:

$$p_\theta(x_{t-1}|x_t) = \mathcal{N}(\mu_\theta(x_t, t), \Sigma_\theta(x_t, t)), \quad (4)$$

where the mean $\mu_\theta(x_t, t)$ can be calculated as a function of $\epsilon(x_t, t)$, and the covariance $\Sigma_\theta(x_t, t)$ can be fixed to a known constant, following [19]. Therefore, DDPMs usually use UNet to estimate the added noise of x_t and optimize the network with a simple loss function:

$$\mathcal{L}_{simple} := E_{t \sim [1, T], x_0 \sim q(x_0), \epsilon \sim \mathcal{N}(0, I)} [||\epsilon - \epsilon_\theta(x_t, t)||^2] \quad (5)$$

In the context of reconstruction-based anomaly detection, our objective is not to create new images from pure noise but to reconstruct the normal image given a noisy input image. Therefore, following [8], [14], [15], we train a denoising model $f_\theta(x_t, t)$ to directly estimate x_0 instead of ϵ_t . Another modification is that we estimate x_0 from x_t at a fixed time step t_{test} when sampling, rather than T steps in traditional DDPM. This simplification significantly decreases the sampling time but not affects the anomaly detection performance. With these two modifications, DDPM can be considered as a Denoising AutoEncoder (DAE) with multi-levels' noises, and can serve as a reconstruction-based anomaly detection method.

pDDPM [14] proposes to conduct the *diffusion* and *reverse* processes only on a patch and use the other region as condition. This technique offers better brain MRI reconstruction by encouraging global context information incorporation. During evaluation, pDDPM reconstructs from noisy patches sampled over the whole image and merge all patches to one final reconstruction. We choose pDDPM to serve as a strong baseline.

B. Fusion Quality Loss

Most existing reconstruction-based anomaly detection methods in Brain MRI, including pDDPM, use ℓ_1 loss to calculate the reconstruction error during training and testing. However, ℓ_1 loss has two main issues in anomaly detection problems: it assumes pixel independence, ignoring spatial relationships, which may prevent the model from learning the intrinsic structure of healthy brains. Additionally, it focuses on intensity discrepancies, which may not capture subtle anomalies with only minor intensity differences from normal parts.

To address these limitations, we propose to assess the reconstruction image quality from a more comprehensive perspective by incorporating the Structural Similarity Index Measure (SSIM).

SSIM is originally constructed as an image quality measure with respect to the human perception rather than absolute differences measured by metrics such as the MSE or Mean Absolute Error (MAE). It measures the similarity between two images x and y from three aspects: luminance $l(x, y)$, contrast $c(x, y)$ and structure $s(x, y)$. The functions are defined as follows:

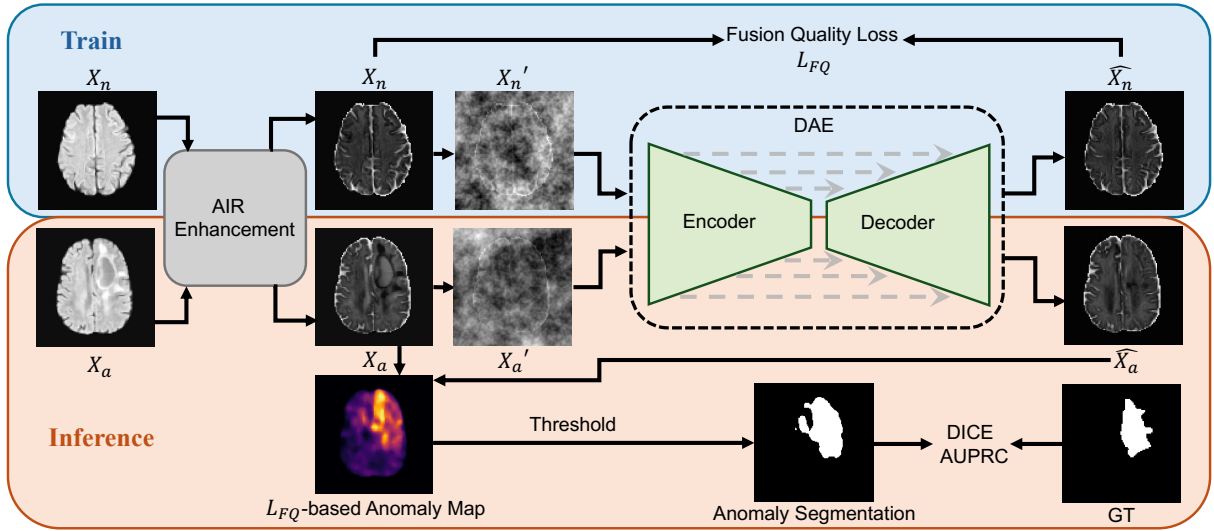


Fig. 2. Overview of our reconstruction-based anomaly detection method using a denoising autoencoder (DAE) as the reconstruction model. During training, the normal dataset X_n is augmented with the proposed AIR enhancement pre-processing strategy and corrupted to form the noisy normal dataset X_n' using simplex noise. The model is then trained by denoising X_n' and minimizing the fusion quality loss L_{FQ} between the reconstruction \hat{X}_n and the original normal dataset X_n . During inference, the abnormal test dataset X_a undergoes the same process. The anomalies in X_a are expected to be poorly reconstructed, resulting in higher values in the L_{FQ} -based anomaly map. The final anomaly map is thresholded for segmentation, with performance measured by DICE and AUPRC.

$$\begin{aligned}
 l(x, y) &= \frac{2\mu_x\mu_y + C_1}{\mu_x^2 + \mu_y^2 + C_1}, \\
 c(x, y) &= \frac{2\sigma_x\sigma_y + C_2}{\sigma_x^2 + \sigma_y^2 + C_2}, \\
 s(x, y) &= \frac{\sigma_{xy} + C_3}{\sigma_x\sigma_y + C_3}
 \end{aligned} \quad (6)$$

where μ_x and μ_y are the means of the images x and y , respectively. σ_x and σ_y are the standard deviations of x and y , respectively. σ_{xy} is the covariance between x and y . C_1, C_2 , and C_3 are small constants to avoid division by zero and to stabilize the computation.

SSIM is then computed as the product of these three components, capturing the perceived quality of the images:

$$\text{SSIM}(x, y) = [l(x, y)]^\alpha [c(x, y)]^\beta [s(x, y)]^\gamma \quad (7)$$

Typically, $\alpha = \beta = \gamma = 1$ and $C_3 = C_2/2$, so the formula simplifies to:

$$\begin{aligned}
 \text{SSIM}(x, y) &= l(x, y) \cdot c(x, y) \cdot s(x, y) \\
 &= \frac{(2\mu_x\mu_y + C_1)(2\sigma_{xy} + C_2)}{(\mu_x^2 + \mu_y^2 + C_1)(\sigma_x^2 + \sigma_y^2 + C_2)}
 \end{aligned} \quad (8)$$

In practice, it is useful to apply SSIM index locally rather than globally for many reasons. The most straightforward one for anomaly detection is that we need a spatially varying quality map of the reconstruction image to localize the anomalies. The local statistics μ_x , σ_x and σ_{xy} are calculated within a $W \times W$ window, moving with a stride S over the entire image.

We set $W = 5$ and $S = 1$ to produce a quality map matching the input shape. The final SSIM loss can be defined as:

$$L_{SSIM}(x, y) = \frac{1 - \frac{1}{K} \sum_{k=1}^K \text{SSIM}(x_k, y_k)}{2} \quad (9)$$

where x_k and y_k are the image contents in the k -th local window, and K is the total number of local windows.

The error at the (i, j) pixel during inference can be defined as:

$$\Lambda(i, j) = \frac{1 - \text{SSIM}(x_{ij}, y_{ij})}{2} \quad (10)$$

where x_{ij} and y_{ij} are the image contents within the local window centered at (i, j) .

By design, SSIM is not particularly sensitive to uniform biases, which can lead to changes in brightness or color shifts. However, SSIM better preserves contrast in high-frequency regions compared to other loss functions as shown in [20]. On the other hand, ℓ_1 loss preserves colors and luminance, treating all errors equally regardless of local structure, but it doesn't maintain contrast as effectively as SSIM.

To capture the best characteristics of both error functions, we propose to combine them and get our final fusion quality loss:

$$L_{FQ} = \alpha L_{SSIM} + (1 - \alpha) L_1 \quad (11)$$

we empirically set $\alpha = 0.84$, as suggested by prior work [20].

C. Average Intensity Ratio Enhancement

After incorporating SSIM loss into the reconstruction assessment metrics, the error is no longer uniformly weighted regardless of the local structure as it is with ℓ_1 loss. Instead, the relationships between regions become more significant. This shift means that the characteristics of a dataset can

significantly influence anomaly detection performance. Moreover, since the new loss function introduces divisive metrics from SSIM, it becomes important to amplify the divisive discrepancies between anomalies and normal regions. Therefore, we propose that an appropriate image processing strategy is necessary to optimize the anomaly detection performance under this new loss function.

We define the average intensity ratio (AIR) between the anomalous and normal regions in an abnormal dataset X as:

$$AIR(X) = \frac{\max(\mu_X^a, \mu_X^n)}{\min(\mu_X^a, \mu_X^n)} \quad (12)$$

where μ_X^a and μ_X^n are the mean values of the anomaly and the normal region, respectively.

Based on the principles of reconstruction-based anomaly detection sketched in Section III-A1, we hypothesize that a higher AIR is important for better anomaly detection performance, mainly for two reasons: 1) A higher AIR suggests a larger discrepancy between the training normal data and the anomalies in the test data, resulting in greater reconstruction errors in the anomalous regions. 2) Since the model aims to reconstruct the normal brain from the noisy anomalies and calculate the difference between the reconstruction and the anomaly as the anomaly score, a higher MIC naturally leads to higher reconstruction errors during evaluation.

During evaluation, existing baselines usually use a validation set $X_{val} \subset X_a$ and the corresponding ground truth Y_{val} to determine hyper-parameters, such as the threshold for binarization. Therefore, it is feasible to perform dataset statistics-based pre-processing operations before training to increase MIC and enhance anomaly detection performance.

In the context of MRI brain anomaly detection, we analyze three modalities from the BraTS21 dataset and find a simple yet effective way that consistently increases the Average Intensity Ratio (AIR) across all datasets used in this paper. Our strategy is based on the following prior statistics calculated on the unhealthy validation set:

- 1) $0 < \mu_X^n < \mu_X^a < 1$ for all three modalities.
- 2) $\mu_X^n > 0.5$ for FLAIR and T1-CE.
- 3) $\mu_X^a < 0.5$ for T2.

Our pre-processing strategy for an image x is then defined as:

$$p(x) = x \cdot \mathbb{I}(u_X^n \leq 0.5) + (1 - x) \cdot \mathbb{I}(0.5 < u_X^n) \quad (13)$$

where \mathbb{I} is an indicator function that returns 1 if the condition inside is true and 0 otherwise. Note that in our experiments, the processing is applied only to the non-zero foreground. We omit this detail here for simplicity in writing. We prove the correctness of our strategy below:

Proof. For FLAIR and T1-CE modality of BraTS21, the prior statistics are:

$$0.5 < \mu_X^n < \mu_X^a < 1 \quad (14)$$

Thus, the pre-processing strategy should be:

$$\begin{aligned} p(x) &= x \cdot 0 + (1 - x) \cdot 1 \\ &= 1 - x \end{aligned} \quad (15)$$

Let \bar{X} denote the dataset after pre-processing. The AIR is then calculated as:

$$\begin{aligned} AIR(\bar{X}) &= \frac{\max(\mu_{\bar{X}}^a, \mu_{\bar{X}}^n)}{\min(\mu_{\bar{X}}^a, \mu_{\bar{X}}^n)} \\ &= \frac{\max(1 - \mu_X^a, 1 - \mu_X^n)}{\min(1 - \mu_X^a, 1 - \mu_X^n)} \\ &= \frac{1 - \mu_X^n}{1 - \mu_X^a} \\ &= 1 + \frac{\mu_X^a - \mu_X^n}{1 - \mu_X^a} \\ &> 1 + \frac{\mu_X^a - \mu_X^n}{\mu_X^n} \\ &= \frac{\mu_X^a}{\mu_X^n} \\ &= \frac{\max(\mu_X^a, \mu_X^n)}{\min(\mu_X^a, \mu_X^n)} = AIR(X) \end{aligned} \quad (16)$$

For T2, the pre-processing is simply:

$$p(x) = x \quad (17)$$

Thus, the AIR remains unchanged:

$$AIR(\bar{X}) = AIR(X) \quad (18)$$

To sum up, with our simple pre-processing strategy, we ensure that for any processed dataset \bar{X} used in our work, the AIR is either maintained or increased, i.e.,

$$AIR(\bar{X}) \geq AIR(X) \quad (19)$$

□

Finally, we refer to our approach as the IQA approach, which includes the proposed Fusion Quality Loss and Average Intensity Ratio Enhancement as its two key components. We apply our IQA approach to the strong baseline pDDPM, resulting in the method we term pDDPM-IQA.

IV. EXPERIMENTS

A. Datasets

We conduct our experiments under both cross-dataset and intra-dataset settings using three publicly available datasets: the Multimodal Brain Tumor Segmentation Challenge 2021 (BraTS21) dataset [23], the multiple sclerosis dataset from the University Hospital of Ljubljana (MSLUB) [24] and the IXI dataset [25].

The BraTS21 dataset contains 1251 brain MRI scans with four modalities (T1, T1-CE, T2, FLAIR). The MSLUB dataset consists of brain MRI scans from 30 multiple sclerosis (MS) patients, each having T1, T2, and FLAIR-weighted scans. The IXI dataset includes 560 pairs of T1 and T2-weighted healthy brain MRI scans.

In the cross-dataset setting, we follow [14] and perform five-fold cross-validation, training the model on healthy T2-weighted scans from IXI and evaluating it on T2-weighted scans from BraTS21 and MSLUB.

TABLE I
COMPARISON WITH BASELINES IN TERMS OF DICE AND AUPRC ON BRA-TS21 AND MSLUB USING T2 MODALITY IN A CROSS-DATASET SETTING. THE MODEL IS TRAINED ON THE IXI DATASET, WHICH CONTAINS ONLY HEALTHY SAMPLES. THE BEST RESULTS FOR A GIVEN METRIC/DATASET ARE BOLDED, AND THE SECOND-BEST ARE UNDERLINED.

Method	BraTS21 (T2)		MSLUB (T2)	
	DICE [%]	AUPRC [%]	DICE [%]	AUPRC [%]
Thresh [21]	19.69	20.27	6.21	4.23
AE [9]	32.87±1.25	31.07±1.75	7.10±0.68	5.58±0.26
VAE [9]	31.11±1.50	28.80±1.92	6.89±0.09	5.00±0.40
SVAE [22]	33.32±0.14	33.14±0.20	5.76±0.44	5.04±0.13
DAE [7]	37.05±1.42	44.99±1.72	3.56±0.91	5.35±0.45
f-AnoGAN [13]	24.16±2.94	22.05±3.05	4.18±1.18	4.01±0.90
DDPM [8]	40.67±1.21	49.78±1.02	6.42±1.60	7.44±0.52
mDDPM [15]	51.31±0.66	57.09±0.94	8.08±0.70	9.06±0.62
pDDPM [14]	49.41±0.66	54.76±0.83	<u>10.65±1.05</u>	<u>10.37±0.51</u>
pDDPM-IQA (ours)	59.45±0.37	62.99±0.37	12.93±0.67	11.51±0.50

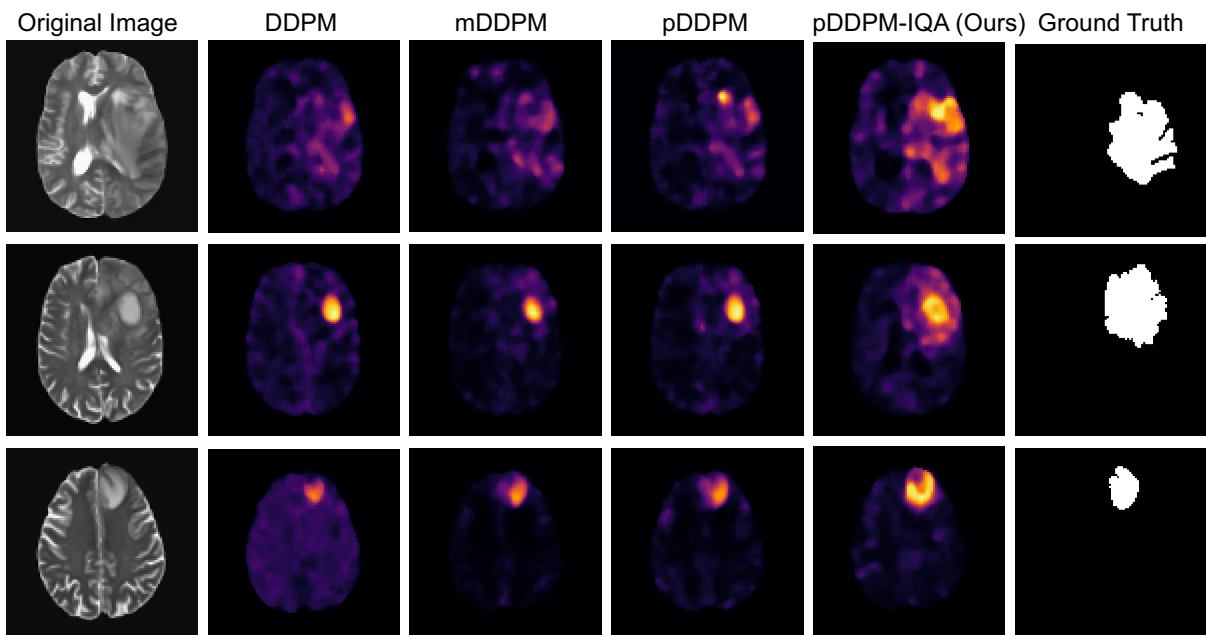


Fig. 3. Qualitative visualization on the BraTS21 test set. Columns 2-5 show anomaly maps from different methods for three samples.

In the intra-dataset setting, we perform five-fold cross-validation on FLAIR and T1-CE scans from BraTS21. For each fold, the slices without tumors are extracted from 60% and 10% of the patients for model training and training-phase validation, respectively. The remaining 30% of the patients are split, with 10% used as the unhealthy validation set and 20% as the test set.

We pre-process all datasets using resampling, skull-stripping, and registration, as described in [14].

B. Implementation Details

We train the model on an NVIDIA A10 GPU using the Adam optimizer, with a learning rate of 1e-4 and a batch size of 32. We use the default settings in pDDPM [14] including using simplex noise as suggested in [8], uniformly sampling noise levels $t \in [1, T]$ with $T = 1000$ during training, and

training for 1600 epochs. For evaluation, we set the noise level t_{test} to 500 for BraTS21 (T2) and 750 for the others.

To enhance the quality of the anomaly map, we employ standard post-processing techniques. First, we apply a median filter with a kernel size of $K_M = 5$ to smooth the anomaly scores, followed by three iterations of brain mask erosion. To determine the optimal binarization threshold, we perform a greedy search on the unhealthy validation set, iteratively calculating Dice scores for various thresholds. The best threshold identified is then used to compute Dice and AUPRC on the unhealthy test set.

C. Comparisons with State-of-the-art Methods

We evaluate the effectiveness of our method against Thresh [21], AE [9], VAE [9], SVAE [22], DAE [7], f-AnoGAN [13], DDPM [8], mDDPM [15] and pDDPM [14], in terms of Dice-

TABLE II
COMPARISON WITH BASELINES IN TERMS OF DICE AND AUPRC ON BRA TS21 USING FLAIR AND T1-CE MODALITIES IN AN INTRA-DATASET SETTING. THE MODEL IS TRAINED ON A SUBSET OF HEALTHY SLICES FROM BRA TS21.

Method	BraTS21 (FLAIR)		BraTS21 (T1-CE)	
	DICE [%]	AUPRC [%]	DICE [%]	AUPRC [%]
DAE [7]	29.12±2.78	28.52±2.91	36.52±0.77	42.10±0.82
DDPM [8]	21.13±2.35	19.89±4.06	30.98±2.57	34.69±2.77
pDDPM [14]	42.63±2.51	46.00±2.75	43.85±2.11	49.06±2.69
pDDPM-IQA (ours)	55.77±1.78	58.27±2.07	46.16±2.09	47.55±2.66

TABLE III
ABLATION STUDY RESULTS EVALUATED ON BRA TS21 USING THE FLAIR MODALITY.

Method	DICE [%]	AUPRC [%]
pDDPM	42.63±2.51	46.00±2.75
pDDPM + L_{SSIM}	47.89±1.51	46.14±1.56
pDDPM + L_{FQ}	50.15±1.08	49.34±1.04
pDDPM + L_{FQ} + AIR \uparrow (pDDPM-IQA)	55.77±1.78	58.27±2.07

TABLE IV
PERFORMANCE OF DDPM-IQA COMPARED TO THE BASELINE DDPM ON BRAIN MRI DATASETS

Method	BraTS21 (T2)		MSLUB (T2)		BraTS21 (FLAIR)		BraTS21 (T1-CE)	
	DICE	AUPRC	DICE	AUPRC	DICE	AUPRC	DICE	AUPRC
DDPM	40.67	49.78	6.42	7.44	21.13	19.89	30.98	34.69
DDPM-IQA	62.02	65.53	11.93	11.17	44.98	48.34	45.40	47.36

Coefficient (DICE) and the average Area Under the Precision-Recall Curve (AUPRC). Results are reported as “mean±std” across five folds.

In Table I, we compare our pDDPM-IQA with state-of-the-art methods on BraTS21 and MSLUB using T2 modality in a **cross-dataset** setting, as adopted in previous studies [14], [15]. Our pDDPM-IQA significantly ($p < 0.05$) outperforms all baseline approaches on both datasets in terms of DICE and AUPRC, with improvements exceeding 10%. Qualitative examples of anomaly maps generated by our method and other models are shown in Fig. 3, demonstrating that pDDPM-IQA provides more precise anomaly detection.

In Table II, we evaluate our method using FLAIR and T1-CE modalities from the BraTS21 dataset in an **intra-dataset** setting. pDDPM-IQA achieves state-of-the-art (SOTA) performance ($p < 0.05$) on the BraTS21 FLAIR dataset, excelling in both DICE and AUPRC. For the BraTS21 T1-CE dataset, pDDPM-IQA also attains SOTA performance in terms of DICE and shows competitive performance in AUPRC, demonstrating its superior capability in accurately detecting and segmenting anomalies.

D. Ablation Study

In Table III, we present the ablation study results on the BraTS21 dataset using the FLAIR modality, highlighting the effectiveness of our proposed fusion quality loss and AIR enhancement pre-processing strategy. The baseline pDDPM

model (using ℓ_1) achieves a DICE score of 42.63% and an AUPRC of 46.00%. Incorporating the L_{SSIM} component slightly improves the results, with a DICE score of 47.89% and an AUPRC of 46.14%, indicating a benefit from structural similarity in anomaly detection. Further enhancement using the fusion quality loss L_{FQ} ($\ell_1 + L_{SSIM}$) yields a notable increase, achieving a DICE score of 50.15% and an AUPRC of 49.34%. Another significant improvement is observed with the addition of the AIR enhancement strategy, where pDDPM-IQA attains a DICE score of 55.77% and an AUPRC of 58.27%. These results demonstrate the substantial impact of the IQA approach, validating their effectiveness in improving the model’s anomaly detection capabilities.

E. Additional Experiments

To verify the generalization of our approach, we apply our IQA approach to another baseline, DDPM, and termed it DDPM-IQA. We evaluate it on BraTS21 T2, MSLUB, BraTS21 FLAIR, and BraTS21 T1-CE, using the same settings as in Table I and Table II. The results in Table IV demonstrate that the proposed IQA approach significantly enhances the performance of DDPM across all datasets, even achieving SOTA performance on the BraTS21 T2 dataset. These findings confirm that our IQA approach is broadly applicable to various reconstruction-based anomaly detection methods in Brain MRI.

V. DISCUSSION AND CONCLUSION

In this study, we investigated reconstruction-based anomaly detection in brain MRI from an image quality assessment (IQA) perspective and proposed a novel IQA approach for medical anomaly detection. Our approach comprises two key components: 1) we introduced the incorporation of SSIM loss into the commonly used ℓ_1 loss, resulting in a fusion quality loss function that more accurately captures the discrepancies between reconstructed and original images. 2) Additionally, we proposed a dataset pre-processing strategy to increase the average intensity ratio (AIR) between normal and abnormal regions.

We apply our IQA approach on a baseline pDDPM model (denoted as pDDPM-IQA in the paper), and it significantly outperforms existing state-of-the-art approaches in terms of DICE and AUPRC across multiple datasets.

It is worth noting that the proposed fusion quality loss and AIR enhancement strategy are specific implementations

under the broader IQA approach. Therefore, further research into new metrics that better assess image quality than the current fusion quality loss could be a valuable direction. Additionally, while our AIR enhancement strategy is tailored to brain MRI images, developing similar strategies for other medical imaging datasets to further improve anomaly detection performance is worth trying.

ACKNOWLEDGMENT

J. C. is funded by the Federal Ministry of Education and Research (Bundesministerium für Bildung und Forschung, BMBF) in Germany under the funding reference 161L0272, and is also supported by the Ministry of Culture and Science of the State of North Rhine-Westphalia (Ministerium für Kultur und Wissenschaft des Landes Nordrhein-Westfalen, MKW NRW).

REFERENCES

- [1] S. Dong, Z. Pan, Y. Fu, Q. Yang, Y. Gao, T. Yu, Y. Shi, and C. Zhuo, "Deu-net 2.0: Enhanced deformable u-net for 3d cardiac cine MRI segmentation," *Medical Image Anal.*, vol. 78, p. 102389, 2022.
- [2] S. Dong, Z. Pan, Y. Fu, D. Xu, K. Shi, Q. Yang, Y. Shi, and C. Zhuo, "Partial unbalanced feature transport for cross-modality cardiac image segmentation," *IEEE Trans. Medical Imaging*, vol. 42, no. 6, pp. 1758–1773, 2023.
- [3] X. Hu, D. Zeng, X. Xu, and Y. Shi, "Semi-supervised contrastive learning for label-efficient medical image segmentation," in *Medical Image Computing and Computer Assisted Intervention - MICCAI 2021 - 24th International Conference, Strasbourg, France, September 27 - October 1, 2021, Proceedings, Part II* (M. de Bruijne, P. C. Cattin, S. Cotin, N. Padoy, S. Speidel, Y. Zheng, and C. Essert, eds.), vol. 12902 of *Lecture Notes in Computer Science*, pp. 481–490, Springer, 2021.
- [4] Z. Pan, J. Chen, and Y. Shi, "Masked diffusion as self-supervised representation learner," 2024.
- [5] C. Baur, B. Wiestler, S. Albarqouni, and N. Navab, "Deep autoencoding models for unsupervised anomaly segmentation in brain MR images," in *Brainlesion: Glioma, Multiple Sclerosis, Stroke and Traumatic Brain Injuries - 4th International Workshop, BrainLes 2018, Held in Conjunction with MICCAI 2018, Granada, Spain, September 16, 2018, Revised Selected Papers, Part I* (A. Crimi, S. Bakas, H. J. Kuijf, F. Keyvan, M. Reyes, and T. van Walsum, eds.), vol. 11383 of *Lecture Notes in Computer Science*, pp. 161–169, Springer, 2018.
- [6] C. Baur, B. Wiestler, S. Albarqouni, and N. Navab, "Bayesian skip-autoencoders for unsupervised hyperintense anomaly detection in high resolution brain mri," in *17th IEEE International Symposium on Biomedical Imaging, ISBI 2020, Iowa City, IA, USA, April 3-7, 2020*, pp. 1905–1909, IEEE, 2020.
- [7] A. Kascenas, N. Pugeault, and A. Q. O’Neil, "Denoising autoencoders for unsupervised anomaly detection in brain MRI," in *International Conference on Medical Imaging with Deep Learning, MIDL 2022, 6-8 July 2022, Zurich, Switzerland* (E. Konukoglu, B. H. Menze, A. Venkataraman, C. F. Baumgartner, Q. Dou, and S. Albarqouni, eds.), vol. 172 of *Proceedings of Machine Learning Research*, pp. 653–664, PMLR, 2022.
- [8] J. Wyatt, A. Leach, S. M. Schmon, and C. G. Willcocks, "Anoddpn: Anomaly detection with denoising diffusion probabilistic models using simplex noise," in *IEEE/CVF Conference on Computer Vision and Pattern Recognition Workshops, CVPR Workshops 2022, New Orleans, LA, USA, June 19-20, 2022*, pp. 649–655, IEEE, 2022.
- [9] C. Baur, S. Denner, B. Wiestler, N. Navab, and S. Albarqouni, "Autoencoders for unsupervised anomaly segmentation in brain MR images: A comparative study," *Medical Image Anal.*, vol. 69, p. 101952, 2021.
- [10] W. H. Pinaya, P.-D. Tudosiu, R. Gray, G. Rees, P. Nachev, S. Ourselin, and M. J. Cardoso, "Unsupervised brain imaging 3d anomaly detection and segmentation with transformers," *Medical Image Analysis*, vol. 79, p. 102475, 2022.
- [11] X. Chen and E. Konukoglu, "Unsupervised detection of lesions in brain mri using constrained adversarial auto-encoders," *ArXiv*, vol. abs/1806.04972, 2018.
- [12] T. Schlegl, P. Seeböck, S. M. Waldstein, U. Schmidt-Erfurth, and G. Langs, "Unsupervised anomaly detection with generative adversarial networks to guide marker discovery," in *Information Processing in Medical Imaging - 25th International Conference, IPMI 2017, Boone, NC, USA, June 25-30, 2017, Proceedings* (M. Niethammer, M. Styner, S. R. Aylward, H. Zhu, I. Oguz, P. Yap, and D. Shen, eds.), vol. 10265 of *Lecture Notes in Computer Science*, pp. 146–157, Springer, 2017.
- [13] T. Schlegl, P. Seeböck, S. M. Waldstein, G. Langs, and U. Schmidt-Erfurth, "f-anogan: Fast unsupervised anomaly detection with generative adversarial networks," *Medical Image Anal.*, vol. 54, pp. 30–44, 2019.
- [14] F. Behrendt, D. Bhattacharya, J. Krüger, R. Opfer, and A. Schlaefer, "Patched diffusion models for unsupervised anomaly detection in brain MRI," in *Medical Imaging with Deep Learning, MIDL 2023, 10-12 July 2023, Nashville, TN, USA* (I. Oguz, J. H. Noble, X. Li, M. Styner, C. Baumgartner, M. Rusu, T. Heimann, D. Kontos, B. A. Landman, and B. M. Dawant, eds.), vol. 227 of *Proceedings of Machine Learning Research*, pp. 1019–1032, PMLR, 2023.
- [15] H. Iqbal, U. Khalid, C. Chen, and J. Hua, "Unsupervised anomaly detection in medical images using masked diffusion model," in *MLMI Learning in Medical Imaging - 14th International Workshop, MLMI 2023, Held in Conjunction with MICCAI 2023, Vancouver, BC, Canada, October 8, 2023, Proceedings, Part I* (X. Cao, X. Xu, I. Rekik, Z. Cui, and X. Ouyang, eds.), vol. 14348 of *Lecture Notes in Computer Science*, pp. 372–381, Springer, 2023.
- [16] P. Bergmann, S. Löwe, M. Fauser, D. Sattlegger, and C. Steger, "Improving unsupervised defect segmentation by applying structural similarity to autoencoders," in *Proceedings of the 14th International Joint Conference on Computer Vision, Imaging and Computer Graphics Theory and Applications, VISIGRAPP 2019, Volume 5: VISAPP, Prague, Czech Republic, February 25-27, 2019* (A. Trémeau, G. M. Farinella, and J. Braz, eds.), pp. 372–380, SciTePress, 2019.
- [17] F. Meissen, J. C. Paetzold, G. Kaissis, and D. Rueckert, "Unsupervised anomaly localization with structural feature-autoencoders," in *Brainlesion: Glioma, Multiple Sclerosis, Stroke and Traumatic Brain Injuries - 8th International Workshop, BrainLes 2022, Held in Conjunction with MICCAI 2022, Singapore, September 18, 2022, Revised Selected Papers* (S. Bakas, A. Crimi, U. Baid, S. Malec, M. Pytlarz, B. Baheti, M. Zenk, and R. Dorent, eds.), vol. 13769 of *Lecture Notes in Computer Science*, pp. 14–24, Springer, 2022.
- [18] F. Behrendt, D. Bhattacharya, L. Maack, J. Krüger, R. Opfer, R. Mieling, and A. Schlaefer, "Diffusion models with ensembled structure-based anomaly scoring for unsupervised anomaly detection," 2024.
- [19] J. Ho, A. Jain, and P. Abbeel, "Denoising diffusion probabilistic models," in *Advances in Neural Information Processing Systems 33: Annual Conference on Neural Information Processing Systems 2020, NeurIPS 2020, December 6-12, 2020, virtual* (H. Larochelle, M. Ranzato, R. Hadsell, M. Balcan, and H. Lin, eds.), 2020.
- [20] H. Zhao, O. Gallo, I. Frosio, and J. Kautz, "Loss functions for image restoration with neural networks," *IEEE Trans. Computational Imaging*, vol. 3, no. 1, pp. 47–57, 2017.
- [21] F. Meissen, G. Kaissis, and D. Rueckert, "Challenging current semi-supervised anomaly segmentation methods for brain MRI," in *Brainlesion: Glioma, Multiple Sclerosis, Stroke and Traumatic Brain Injuries - 7th International Workshop, BrainLes 2021, Held in Conjunction with MICCAI 2021, Virtual Event, September 27, 2021, Revised Selected Papers, Part I* (A. Crimi and S. Bakas, eds.), vol. 12962 of *Lecture Notes in Computer Science*, pp. 63–74, Springer, 2021.
- [22] F. Behrendt, M. Bengs, D. Bhattacharya, J. Krüger, R. Opfer, and A. Schlaefer, "Capturing inter-slice dependencies of 3d brain mri-scans for unsupervised anomaly detection," in *Medical Imaging with Deep Learning*, 2022.
- [23] U. Baid, S. Ghodasara, S. Mohan, M. Bilello, E. Calabrese, E. Colak, K. Farahani, J. Kalpathy-Cramer, F. C. Kitamura, S. Pati, *et al.*, "The rsna-asnr-miccai brats 2021 benchmark on brain tumor segmentation and radiogenomic classification," *arXiv preprint arXiv:2107.02314*, 2021.
- [24] Z. Lesjak, A. Galimzianova, A. Koren, M. Lukin, F. Pernus, B. Likar, and Z. Spiclin, "A novel public MR image dataset of multiple sclerosis patients with lesion segmentations based on multi-rater consensus," *Neuroinformatics*, vol. 16, no. 1, pp. 51–63, 2018.
- [25] <https://brain-development.org/ixi-dataset/>.